

# ***Bifurcation analysis of thermoacoustic instability in a horizontal Rijke tube***

**Priya Subramanian<sup>1</sup>, Sathesh Mariappan<sup>2</sup>, R. I. Sujith<sup>\*,3</sup> and Pankaj Wahi<sup>4</sup>**

<sup>1, 2, 3</sup>*Department of Aerospace Engineering, Indian Institute of Technology Madras  
Chennai-600036, India*

<sup>4</sup>*Department of Mechanical Engineering, Indian Institute of Technology Kanpur  
Kanpur-201086, India*

Received on 5<sup>th</sup> April 2010; Revised submission on 13<sup>th</sup> August 2010, Accepted on 4<sup>th</sup> November 2010

A bifurcation analysis of the dynamical behavior of a horizontal Rijke tube model is performed in this paper. The method of numerical continuation is used to obtain the bifurcation plots, including the amplitude of the unstable limit cycles. Bifurcation plots for the variation of nondimensional heater power, damping coefficient and the heater location are obtained for different values of time lag in the system. Subcritical bifurcation was observed for variation of parameters and regions of global stability, global instability and bistability are characterized. Linear and nonlinear stability boundaries are obtained for the simultaneous variation of two parameters of the system. The validity of the small time lag assumption in the calculation of linear stability boundary has been shown to fail at typical values of time lag of system. Accurate calculation of the linear stability boundary in systems with explicit time delay models, must therefore, not assume a small time lag assumption. Interesting dynamical behavior such as co-existing multiple attractors, quasiperiodic behavior and period doubling route to chaos have been observed in the analysis of the model. Comparison of the linear stability boundaries and bifurcation behavior from this reduced order model are shown to display trends similar to experimental data.

## **1. INTRODUCTION**

Combustion instability is a plaguing problem in the development of combustors for rockets and gas turbines used in jet engines and power generation [1]. Fluctuations in heat release rate arise due to acoustic fluctuations. They can further act as a source of acoustic fluctuations and the coupled system can reach self-sustained large amplitude oscillations. Combustion instability is caused when the fluctuating heat release rate and the acoustic field form a positive feedback loop.

Traditionally, linear stability analysis is performed by examining the spectrum of the linearized system. When all the eigenvalues of the system are in the left half of the complex plane, the eigenmodes of the system have negative growth rates and therefore

---

Prof. Wolfgang Polifke served as the sole independent editor for this paper.

\*Corresponding author: sujith@iitm.ac.in

the system is linearly stable. If one or more of the eigenvalues lie on the right half of the complex plane, correspondingly the eigenmodes have positive growth rates and the system is linearly unstable. In a linearly unstable system, any infinitesimal initial perturbation grows exponentially and asymptotically reaches another state different from the initial state. A linearly stable system can also exhibit subcritical transition to instability and asymptotically reach another state for suitable initial conditions. This type of subcritical transition to instability from a finite amplitude initial condition is called triggering [2].

Triggering has been exhibited in solid rocket motors [2] and also in Rijke tube [3]. Triggering can cause a system which is linearly stable to become unstable in the presence of a finite amplitude disturbance. Therefore in systems exhibiting subcritical transition to instability, it is important to determine the nonlinear stability boundaries and the limit cycle characteristics. As linear stability analysis cannot predict the limit cycle characteristics, nonlinear stability analysis or bifurcation analysis of thermoacoustic instability is necessary.

We will perform nonlinear stability analysis of a thermoacoustic system by using a simple model for thermoacoustic oscillations in a horizontal Rijke tube [5] that displays the essential features. Rijke tube is an acoustic resonator tube, which consists of a heat source (in the present case, an electrical heater), positioned at some axial location. A mean flow is maintained at a desired flow rate using a blower. A correlation between the heat release rate fluctuations at the heater location and the acoustic velocity fluctuations at the heater [10] is used to model the fluctuating heat release rate from the heater in the Rijke tube [5]. In the present paper, we use this model problem to understand the nonlinear dynamics in a Rijke tube. Approaches used to study instability in a Rijke tube are briefly reviewed below.

### **1.1. Thermoacoustic instability in a Rijke tube**

Self-sustained thermoacoustic oscillations are observed in the Rijke tube when the heater is positioned at certain axial locations of the tube and beyond some threshold power level. Linear models for the unsteady heat release rate due to the acoustic velocity fluctuations were used to calculate linearly unstable locations along the Rijke tube [6]. The stability thus predicted is the linear stability of the system; i.e. the stability of oscillations in the asymptotic time limit for small amplitude oscillations. Therefore this method cannot predict finite amplitude effects such as triggering instabilities and the limit cycle characteristics. Estimation of the amplitude of acoustic oscillations during limit cycle is important from the design point of view for gas turbines. For this, the nonlinearity in the heat release rate response of the heater has to be included [7] in the analysis. CFD based analysis was also used to study Rijke tube oscillations with the heat source being considered as a heated flat plate [8] or as flow over a cylinder [9]. The transfer functions obtained from CFD simulations of flow around cylinders [7] have been used to study the bifurcation behavior in a Rijke tube [3, 4].

In most of the cases, solving the governing equations to obtain the unsteady heat transfer from the heater is computationally expensive. For those cases, a low order model is used to simulate the nonlinear response of the heater. A low order time lag

model based on a correlation for the heat release rate given by Heckl [10] has been used to model the dynamics of the heater [5]. The Rijke tube model thus obtained is a physical model which is based on experimental observations. In this paper, results from the present low order model are compared with experimental results obtained by Matveev [4].

This above mentioned low order model is seen to retain the diverse dynamical behavior of the thermoacoustic instability in a Rijke tube and exhibits nonlinear phenomena such as subcritical transition to instability and limit cycles. Bifurcation analysis of low dimensional models of systems has been studied using many techniques for combustion instabilities in combustion chambers [11, 12]. This analysis can be used to identify the nature of the transition to instability and to characterize the finite amplitude oscillations produced. A brief review of the techniques used in bifurcation analysis is given below.

## **1.2. Techniques for bifurcation analysis**

The approach of obtaining bifurcation diagrams by systematic variation of parameter and tracking direct time integration was used by Moeck [13], Mariappan & Sujith [9]. This method is computationally expensive. Moreover, the basins of attraction obtained for the limit cycle and the steady state remain specific to the type of initial condition applied, making it not suited for systems which exhibit pulsed instability [12]. Accurate knowledge of the basins of attraction can be critical in understanding the global dynamics of the system [14].

Numerical continuation [12, 15] is an alternate approach to obtain bifurcation diagram from a numerical model. This method aims to solve a set of parameterized nonlinear equations iteratively given an initial guess for the state of the system. Solutions which satisfy the set of equations and which are additionally connected to a given state of the system are tracked for a given smooth variation of one or more parameters. Bifurcations are identified by including multiple test functions which change sign at the critical value of the parameter. This method has the advantage that once a stationary or periodic solution has been computed, the dependence of the solution on the variation of a parameter is obtained very efficiently as compared with the other methods described earlier. It can also be used to compute unstable limit cycles.

Jahnke & Culick [11] used the continuation method to obtain the amplitudes of longitudinal acoustic modes in a combustion chamber. They obtained bifurcation plots for different number of normal modes of the combustion chamber. Pitchfork bifurcations leading to limit cycles and torus bifurcation leading to quasiperiodic motions were observed in this analysis. Burnley [16] investigated the stability of a combustion chamber using numerical continuation and the effect of combustion noise on the stability of the system. Reduced order models for the combustion chambers have been solved by the framework of expanding the pressure and velocity fields in terms of modal or basis functions. Ananthkrishnan *et al.* [12] examined the issue of modal truncation and established the number of modes required to accurately capture the dynamics of the system. Control of a simple one-mode model of the thermoacoustic system model was performed by Fannin *et al.* [17].

However, in numerical continuation, the different types of equations encountered in models of physical systems require special attention during the analysis stage. As an example, numerical continuation methods used for models containing delay differential equations must be capable of handling time delay systems. This is essential in the present paper as the low order model used for the Rijke tube contains an explicit delay term.

Numerical continuation methods for delay systems have been developed by Engelborghs & Roose [18, 19]. Their software called DDE-BIFTOOL, has been used to obtain the bifurcation results in the present paper. A system of delay differential equations is infinite-dimensional and has an infinite number of roots associated with the steady state which govern its stability. However, only a finite number of them have real part greater than a specified value and hence finitely many of the dominant roots govern the dynamics. In DDE-BIFTOOL [18] the steady state of the system is evaluated iteratively using a Newton-Raphson scheme and the obtained steady state is then used to continue the solution curve for variations of one or more chosen parameters of the system.

The dominant roots (with real parts greater than a value specified by the user) associated with these steady states are then evaluated numerically and bifurcation points are detected. To get the periodic solutions of the system, an appropriate boundary value problem wherein the solution of the governing equations of the system satisfies the constraint of continuity of states at two time instants one time-period apart is solved using an orthogonal collocation method [19]. Branches of periodic solutions with variations of relevant parameters are obtained analogous to the branches of the fixed points and their stability is estimated by calculating the dominant Floquet multipliers. The main objective of the present paper is to determine the bifurcation behavior of the Rijke tube model including the unstable limit cycles using DDE-BIFTOOL.

The stability boundaries of the steady solution in different parameter spaces will also be obtained and the results validated with time marching solutions of the system. Significant system parameters to be varied are the non-dimensional heater power ( $K$ ), location of heater ( $x_f$ ), damping coefficient ( $c_1$ ) and the time lag ( $\tau$ ). The rest of the paper is organized as follows. Section 2 describes the low order model for the Rijke tube and the formulation used in numerical continuation. Analysis of the results obtained from numerical continuation is explained in section 3. The results of bifurcation analysis using numerical continuation for various parameters and comparison of numerical results with experimental data are summarized in section 4. Section 5 lists the conclusions of the present work and presents the scope for future work.

## 2. MODEL FOR RIJKE TUBE

The Rijke tube model used in the present paper closely follows Balasubramanian & Sujith [5] and is for the geometry shown in Figure 1. This model uses the zero Mach number approximation [20] and is governed by the non-dimensional linearized momentum and energy equations for the acoustic field as given below in Eqns (1) and (2). The scales for non-dimensionalisation are as given in Eqn (3).

$$\gamma M \frac{\partial u'}{\partial t} + \frac{\partial p'}{\partial x} = 0, \quad (1)$$

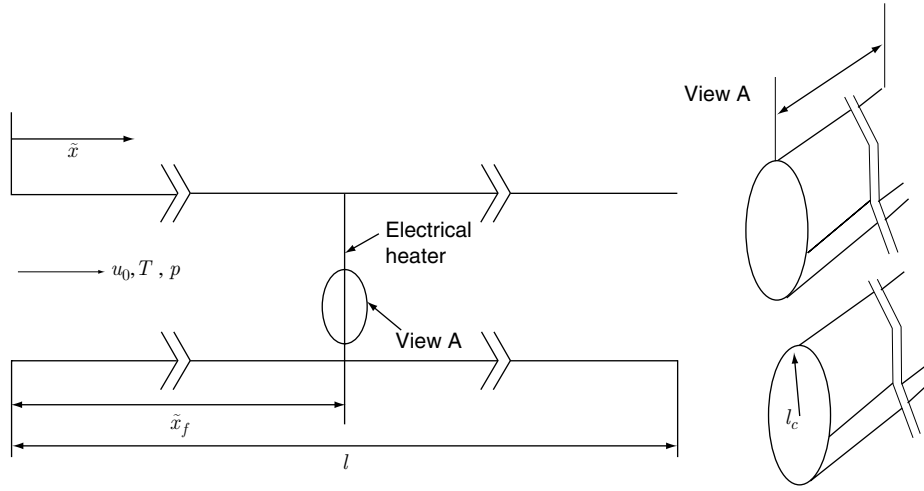


**Figure 1:** Configuration of a horizontal Rijke tube with an electric heater as source.

$$\frac{\partial p'}{\partial t} + \gamma M \frac{\partial u'}{\partial x} + \zeta p' = (\gamma - 1) \dot{Q}'(t) \delta(x - x_f). \quad (2)$$

$$x = \frac{\tilde{x}}{l}; t = \frac{c_0}{l} \tilde{t}; u' = \frac{\tilde{u}'}{u_0}; p' = \frac{\tilde{p}'}{\bar{p}}; M \frac{u_0}{c_0}. \quad (3)$$

In this model,  $x$  is the distance along the axial direction,  $l$  is the length of the duct and  $t$  is time. The flow has a steady state velocity  $u_0$ , pressure  $\bar{p}$  and temperature  $\bar{T}$  as shown in the figure 1, with  $u'$  as acoustic velocity and  $p'$  as acoustic pressure. When  $\gamma$  is the ratio of specific heats of the medium, the speed of sound is calculated as  $c_0$  and  $M$  is the Mach number of the mean flow. Additionally,  $\zeta$  is the damping coefficient and  $\dot{Q}'$  is the heat release rate fluctuations per unit area due to the electrical heater. Quantities with tilde are dimensional and those without tilde are non-dimensional.

The response of the heat transfer from the wire filament to acoustic velocity fluctuations is quantified using the correlation given by Heckl [10]. This correlation quantifies the quasi-steady heat transfer from a heated cylinder to the flow around it [21]. A time lag is introduced in the correlation in order to include for the thermal inertia of the heat transfer [10]. The heat release rate fluctuations can then be rewritten in terms of the acoustic velocity fluctuations as given in Eqn (4).

$$\dot{Q}'(t) = \frac{2L_w(T_w - \bar{T})}{S\sqrt{3}c_0\bar{p}} \sqrt{\pi\lambda C_V u_0 \bar{\rho} l_c} \left[ \sqrt{\left| \frac{1}{3} + u'_f(t - \tau) \right|} - \sqrt{\frac{1}{3}} \right]. \quad (4)$$

The energy equation can be modified as given below by including the correlation for heat release rate fluctuations:

$$\begin{aligned} \frac{\partial p'}{\partial t} + \gamma M \frac{\partial u'}{\partial x} + \zeta p' = (\gamma - 1) \frac{2L_w(T_w - \bar{T})}{S\sqrt{3c_0\bar{\rho}}} \sqrt{\pi\lambda C_V u_0 \bar{\rho} l_c} \\ \times \left[ \sqrt{\frac{1}{3} + u'_f(t - \tau)} - \sqrt{\frac{1}{3}} \right] \delta(x - x_f) \end{aligned} \quad (5)$$

where  $l_c$ ,  $L_w$  and  $T_w$  are the radius, length and temperature of the wire respectively,  $S$  is the cross sectional area,  $\bar{\rho}$  is the mean density,  $\lambda$  is the thermal conductivity and  $C_V$  is the specific heat at constant volume of the medium within the duct.

The non-dimensional partial differential equations Eqn (1) and Eqn (5) can be reduced to a set of ordinary differential equations by expanding the acoustic variables in terms of basis functions using the Galerkin technique [22]. The Galerkin basis functions chosen here are the natural acoustic modes of the duct in the absence of a heater. The duct modes in the absence of the heater have non-dimensional frequencies  $f = 0.5j$  and time periods  $T = 2/j$  for  $j = 1$  to  $N$ . In the following expressions  $k_j = j\pi$  refers to the non-dimensional wave number and  $\omega_j = j\pi$  refers to the non-dimensional angular frequency of the  $j^{\text{th}}$  duct mode.

$$u' = \sum_{j=1}^N \cos(k_j x) U_j(t), \quad (6)$$

$$p' = \gamma M \sum_{j=1}^N \sin(k_j x) P_j(t). \quad (7)$$

$$\dot{U}_j + k_j P_j = 0, \quad (8)$$

$$\dot{P}_j + 2\zeta_j \omega_j P_j - k_j U_j = K \left[ \sqrt{\frac{1}{3} + u'_f(t - \tau)} - \sqrt{\frac{1}{3}} \right] \sin(k_j x_f). \quad (9)$$

Here,  $\zeta = 2\omega_j \zeta_j$  is the expression for frequency dependent damping where  $\zeta_j$  is given by Matveev [3, 23] as shown in Eqn (10) and  $c_1$  and  $c_2$  are the damping coefficients which can be varied and which control the amount of damping in the system.

$$\zeta_j = \frac{1}{2\pi} \left( c_1 \frac{\omega_j}{\omega_1} + c_2 \sqrt{\frac{\omega_1}{\omega_j}} \right), \quad (10)$$

The resulting set of equations as given in Eqns (8) and (9) are evolved in time. Here, the expression for the non-dimensional heater power ( $K$ ) is given by,

$$K = \frac{4(\gamma - 1)L_w}{\gamma M c_0 \bar{p} S \sqrt{3}} (T_w - \bar{T}) \sqrt{\pi \lambda C_V u_0 \bar{\rho} l_c}. \quad (11)$$

The equations can be simplified by expanding the term under the square root in Eqn (9) under the assumptions of small acoustic velocity at the flame ( $u_f'$ ) and small time lag ( $\tau$ ). The resulting equation, valid in the limit of small time lag, is written as given below in Eqn (12).

$$\dot{P}_j + 2\zeta_j \omega_j P_j - k_j U_j = K \frac{\sqrt{3}}{2} \left[ \sum_{i=1}^N \cos(k_i x_f) U_i(t) + \tau \sum_{i=1}^N \cos(k_i x_f) P_i(t) \right] \sin(k_j x_f). \quad (12)$$

### 3. ANALYSIS

#### 3.1. Steady-state equilibrium and linear stability analysis

The effect of infinitesimal perturbations on the evolution of the system about a steady state is investigated in linear stability analysis. If the evolution moves away from the steady state, the system is unstable and if the evolution approaches the steady state, then the system is stable. This refers to the local analysis of the stability of the system near a steady state. On the other hand, nonlinear stability analysis follows the effect of a finite amplitude perturbation to the system and is used to characterize the resulting asymptotic state.

As an initial step in performing the stability analysis of a steady-state equilibrium solution for given parameter values, the steady state of the system for the given set of parameters has to be calculated. This calculation is done in DDE-BIFTOOL using the Newton's method. Next linear (local) stability of the obtained equilibrium is identified by examining the eigenvalues of the system linearized around the equilibrium. If all the eigenvalues lie on the left half plane, the equilibrium is linearly stable to small perturbations. When one or more eigenvalues of the linearized system lie on the right half plane, the system is said to be linearly unstable. Stability properties of the equilibrium is therefore changed when the real part of the most dominant eigenvalue crosses zero as some relevant parameter of the system is varied. The value of the parameter at which the real part of the most dominant eigenvalue is zero is called the bifurcation point.

The behavior of the system changes as this value of the parameter is crossed since the equilibrium solution loses stability. New steady states emerge from the bifurcation point depending on the type and nature of the bifurcation to be discussed in the next section. A bifurcation point is located in DDE-BIFTOOL by continuing the equilibrium solution branch with a variation in the relevant parameter and studying the spectrum of the first few dominant eigenvalues.

Once a bifurcation point is located with respect of one parameter, the bifurcation point itself is continued with a variation in a second relevant parameter of the system. The resulting branch of bifurcation points gives us the linear stability boundary which separates regions in the relevant parameter space with linearly stable and unstable

equilibrium. This stability boundary is a hyper-surface in the space of all the free parameters of the system, but is most conveniently represented by a curve in several appropriate two-dimensional projections. A typical stability boundary for free variation of the heater location and the time lag of the system is shown in Figure 2.

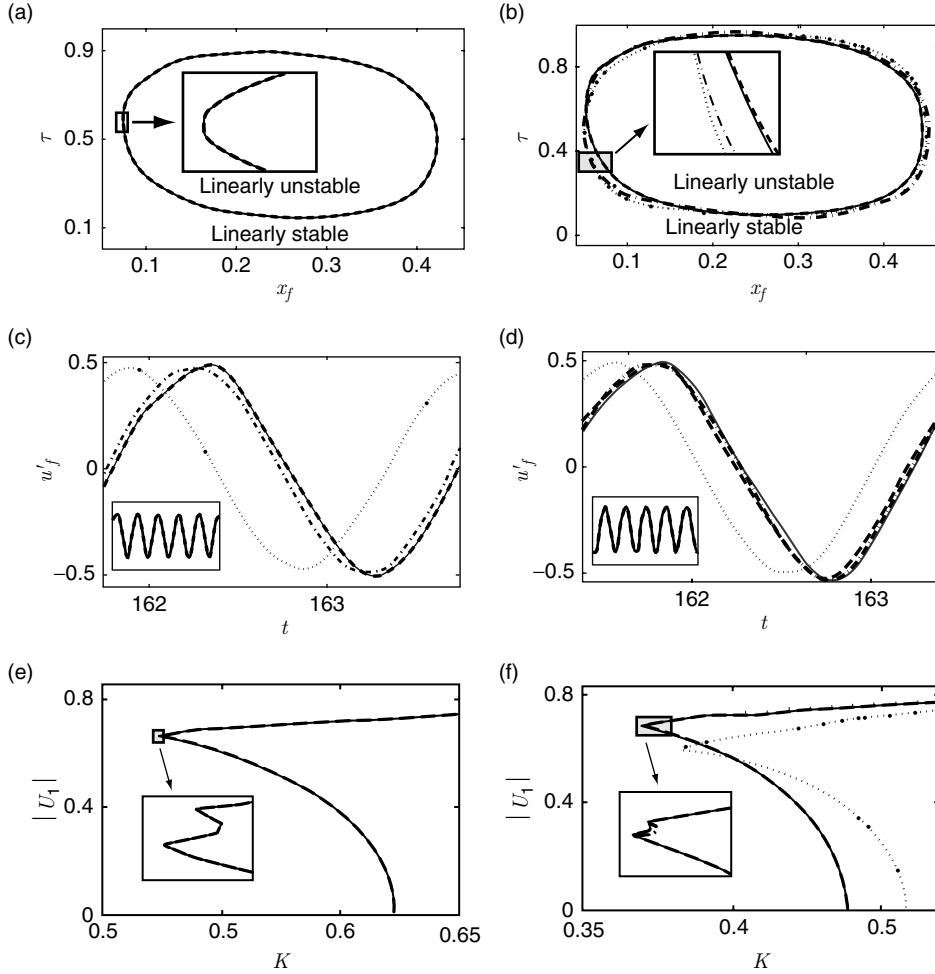


**Figure 2:** Modal convergence of linear stability boundary between  $x_f$  and  $\tau$  with (a)  $c_1 = 0.1, c_2 = 0.06$  and  $K = 0.8$  (b)  $c_1 = 0.05, c_2 = 0.06$  and  $K = 0.8$ . In this Figure,  $\cdots \cdots N = 1$ ,  $\cdots - \cdots N = 2$ ,  $- - - N = 9$  and  $- N = 10$ . Comparison of limit cycle amplitude from time evolutions with different number of acoustic Galerkin modes ( $N$ ) with  $x_f = 0.3$  and  $\tau = 0.2$  (c) for case shown in 2(a) and (d) for case shown in 2(b). Comparison of bifurcation plots for variation of non-dimensional heater power ( $K$ ) with different number of acoustic Galerkin modes ( $N$ ) (e) for system in 2(a) (f) system in 2(b). Grey areas are enlarged in inset figures to show convergence with increase in number of modes.



Figure 2 shows that for the chosen set of fixed parameter values for the damping and the heater power, the system is linearly unstable for a chosen range of heater locations ( $x_f$ ) depending on the time lag  $\tau$  of the system and vice versa. For very low and reasonably large values of  $\tau$  like  $\tau < 0.15$  and  $\tau > 0.85$  in Figure 2(a), the system is linearly stable for any heater location. Only in the range  $0.15 < \tau < 0.85$ , the equilibrium solution can become unstable depending on the heater location.

The number of Galerkin modes required to accurately capture the linear and nonlinear behavior of the system is termed as modal convergence in the caption of Figure 2. In this figure, the stability boundary for different number of acoustic Galerkin modes from 1 mode to 10 modes show little variation for the case shown in 2(a) while for the case shown in 2(b) with lesser damping 10 modes are required to capture the linear stability boundary accurately.

In the remainder of this paper, we will use 10 Galerkin modes only and will not reduce our damping coefficient  $c_1$  less than 0.1. In the next section, we discuss limit cycles obtained using the nonlinear analysis and establish the convergence of the general solution of the system for 10 Galerkin modes.

### 3.2. Numerical simulation, limit cycles and nonlinear analysis

The bifurcation points at the linear stability boundaries obtained in the previous section are associated with a pair of complex conjugate eigenvalues crossing the imaginary axis and accordingly there is a Hopf bifurcation. At the Hopf bifurcation point, the steady state loses stability and becomes unstable, and isolated periodic solutions called limit cycles emerge. The stability of the emerging branch of limit cycles decides the type or nature of the Hopf bifurcation. The two types are shown in Fig. 3. If the limit cycles are unstable, as shown in Fig. 3(a), the branch of unstable limit cycles forms a region of bistability where the steady solution is stable to small perturbations but is unstable to large perturbations. However this branch of unstable limit cycle might undergo a fold bifurcation and stabilize. For values below the fold point the steady solution is stable to perturbations of any magnitude and hence are globally stable. Therefore in the case of a subcritical bifurcation, the linear (local) and nonlinear (global) stability boundaries are different. This behavior is called a subcritical Hopf bifurcation. If however the limit cycles are stable as shown in Fig. 3(b), the system smoothly evolves from a stable steady solution to an unstable steady solution with progressively increasing limit cycle amplitudes. This type of bifurcation is called a super-critical Hopf bifurcation.

We first check the existence of limit cycles in our model and the convergence of the number of acoustic Galerkin modes. For this the time evolutions of the system with different number of acoustic modes for system parameters in the linearly unstable region are compared in Figs. 2(c-d). It can be seen from Figs. 2(c) that there is a limit cycle and also that the amplitude of the limit cycle shows very little variation with an increase in the number of acoustic Galerkin modes. The variation in the phase of the various solutions can be attributed to initial conditions. In fact, the difference in the solutions with different numbers of acoustic modes is not visible when the phase difference is compensated. This feature can be seen more easily from Figure 2(e) wherein we have plotted the variation of the amplitudes of the first Galerkin mode with a variation in the heater power  $K$ . In fact the measure used to quantify the asymptotic

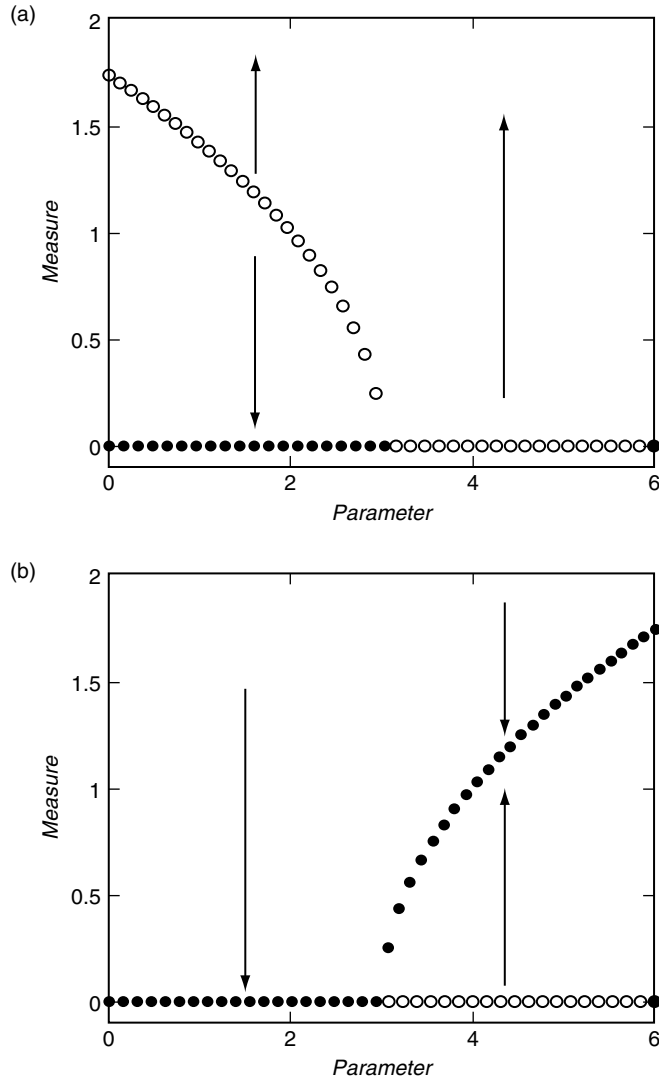


**Figure 3:** Bifurcation behavior of a *Measure* for the variation of a *Parameter* near a (a) Subcritical and (b) Super-critical Hopf bifurcation. • indicate stable solutions and ○ indicate unstable solutions.

state ( $t \rightarrow \infty$ ) of the system in Figure 2(e) is the difference between the maximum and minimum value ( $|U_1|$ ) of the non-dimensional first acoustic velocity mode.

The amplitudes of the limit cycles in Figure 2(e) are obtained using continuation of the limit cycles using DDE-BIFTOOL. In this Figure, the equilibrium is stable for  $K < 0.625$  and small-amplitude limit cycles originating from the Hopf bifurcation point

also exists in this region. These limit cycles are unstable and the Hopf bifurcation is subcritical in nature. As the amplitude of these limit cycles increase in magnitude, these limit cycles stabilize through a ‘turning point’ or ‘fold’ bifurcation. The unstable branch of limit cycles turns around at around  $K = 0.523$  and in the region  $0.523 < K < 0.625$ , a stable equilibrium, an unstable small-amplitude limit cycle and a large-amplitude stable limit cycle coexist. This is the range of ‘bistability’ [24, 25] where the equilibrium is only locally stable and large amplitude disturbances grow to limit cycles.

It is to be noted that the amplitudes of the limit cycles shown in the bifurcation plots are only the amplitudes of the first Galerkin mode in the asymptotic state. Initial conditions reach either the stable limit cycle or the steady state depending on the magnitude of the perturbation relative to the amplitudes of the unstable limit cycles only if the initial condition given has nonzero component only in the first Galerkin mode. Therefore the unstable limit cycle shown in the bifurcation diagrams are not representative of the basin boundaries but represent only the triggering amplitudes for the above mentioned kind of initial conditions. The basin boundaries are formed by the stable manifolds of these unstable limit cycles and they lie in a high-dimensional space. As mentioned earlier, below the fold bifurcation point, i.e., for  $K < 0.523$  the equilibrium is globally stable to any perturbations.

When the damping coefficients are reduced, the change in the amplitudes of the limit cycles with an increase in the number of acoustic Galerkin modes is more significant as can be seen from Figures 2(d) and 2(f). Both the location of the Hopf bifurcation point and the location of the fold bifurcation point are seen to change when the number of modes is increased from 1 to 2 suggesting that a single mode Galerkin projection is largely inadequate to capture the true stability information.

These changes decrease with an increase in the number of modes and the difference in the solution with 9 and 10 acoustic modes is almost negligible again emphasizing the convergence of the model with 10 acoustic modes in the Galerkin projection. For a model with 10 acoustic modes, an addition of more Galerkin modes changes the limit cycle amplitude of the acoustic velocity by less than 1.4%. Therefore, in all calculations considered henceforth, a model with 10 Galerkin modes is used to ensure convergence in the number of acoustic Galerkin modes for the linear and nonlinear stability analysis.

We noted in Figs. 2(e) and 2(f) that a subcritical Hopf bifurcation happens when the non-dimensional heater power is varied as the free parameter. This will also happen with variation in any other free parameter of the system as it is an inherent property of the nonlinearity present in the system. To justify our claim, we present a crude qualitative analysis which will be substantiated with a more rigorous analysis along the lines of Saha *et al.* [26] in our future work. The nature of the bifurcation associated with a source term nonlinearity of the form  $(1 \pm X)^\alpha$ , where  $X$  is the state variable and  $\alpha$  is a real number can be identified by expanding the nonlinearity in a series about small  $X$  and dropping higher order terms. A binomial expansion of the above expression results in the following equation.

$$1 \pm \alpha X + \frac{\alpha(\alpha-1)}{2!} X^2 \pm \frac{\alpha(\alpha-1)(\alpha-2)}{3!} X^3 + \dots \quad (13)$$

In the above expression, the signs of the first and the third order terms are seen to be same when  $0 < |\alpha| < 1$  and  $|\alpha| > 2$ . The signs will be different when the value of  $\alpha$  lies between  $1 < |\alpha| < 2$ . The relative signs of the first and the third order term dictates the nature of the bifurcation. Whenever these terms have the same sign, the bifurcation is subcritical while it is supercritical when these terms have different signs. This result has been obtained in the context of machine tool vibrations by Kalmar-Nagy *et al.* [27] and Wahi and Chatterjee [28] for  $\alpha = 3/4$ . In the model for the heat release rate fluctuations in a Rijke tube,  $\alpha = 1/2$ , which implies that this model will exhibit subcritical Hopf bifurcation.

We had noted in our previous discussion in this section that there are multiple co-existing solutions in the range of the free parameter values between the Hopf point and the fold point. A stable steady state and a pair of stable and unstable limit cycles are seen to co-exist which is a general feature of systems exhibiting subcritical Hopf bifurcation followed by a fold bifurcation which gives rise to a branch of stable limit cycle solutions. Depending on the initial condition, the system will asymptotically reach a steady state or a limit cycle. This range of parameters has two possible asymptotic states and is hence called the region of bistability. The region of bistability for the variation of non-dimensional heater power and the time lag is shown in Figure 4.

In this figure the linear stability boundary is the locus of the Hopf points, i.e. when the non-dimensional power is larger than this value, an infinitesimal perturbation is sufficient to destabilize the steady state of the system. Similarly, the nonlinear stability boundary is the locus of the fold points, i.e. when the non-dimensional power is below this value, the steady state of the system is stable to any finite amplitude perturbation. In the region between the two curves (the bistable region), a finite amplitude perturbation is required to destabilize

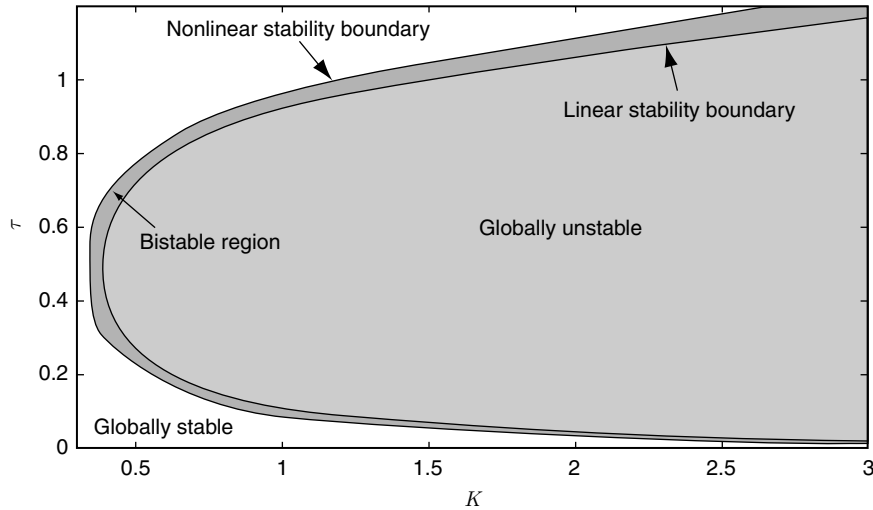


**Figure 4:** Region of bistability obtained for the bifurcation between non-dimensional heater power ( $K$ ) and time lag ( $\tau$ ) with the other system parameters being  $c_1 = 0.1$ ,  $c_2 = 0.06$  and  $x_f = 0.3$ .

the system from the unperturbed state. The nonlinear stability boundary can also be called as the ‘triggered’ or ‘pulsed’ instability boundary as it marks the beginning of the triggering.

It can be seen from this figure that the bistability region is much smaller for small time lags and it increases with an increase in the time lag in the system. Hence, the effect of the nonlinearity introduced by the heating is more profound for larger time lags which roughly corresponds to smaller speeds of mean flow in the tube. (Refer Eqn 14)

## 4. RESULTS & DISCUSSIONS

### 4.1. On the effect of the small time lag assumption

The delay differential equations governing the Rijke tube system are linearized about  $\tau = 0$  to get ordinary differential equations which are valid for small time lags. The corresponding set of equations in the matrix form  $dX/dt = LX$  is given in Balasubramanian & Sujith [5]. This matrix  $L$  can be used to calculate the eigenvalues of the system with small time lag assumption and the value of the parameters when the system becomes unstable can be noted as the stability boundary. This approximate stability boundary is compared with the exact stability boundary predicted by the system of delay differential equations given by Eqns (8) and (9) in Figure 5.

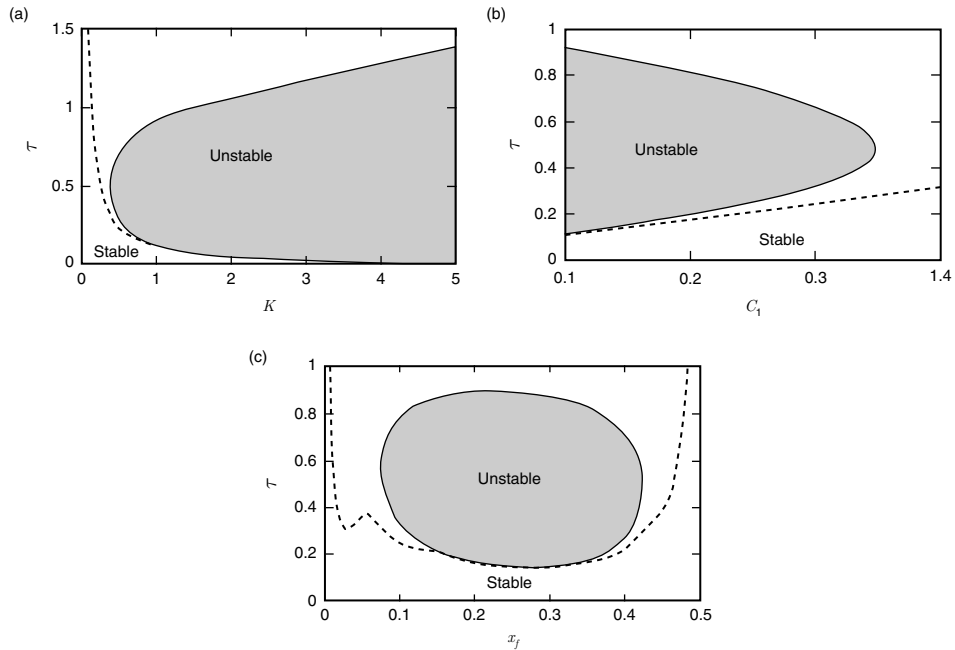


**Figure 5:** Comparison of stability boundary obtained with --- and without — the small time lag assumption between (a) non-dimensional heater power ( $K$ ) and time lag ( $\tau$ ) with the other system parameters being  $c_1 = 0.1$ ,  $c_2 = 0.06$  and  $x_f = 0.3$ . (b) damping coefficient ( $c_1$ ) and time lag ( $\tau$ ) for  $c_2 = 0.06$ ,  $K = 1$  and  $x_f = 0.3$  (c) location of heater ( $x_f$ ) and time lag ( $\tau$ ) with the other system parameters being  $c_1 = 0.1$ ,  $c_2 = 0.06$  and  $K = 0.8$ .

The linear stability boundaries showing the variation of the critical nondimensional heater power  $K$ , damping coefficient  $c_1$  and the heater location  $x_f$  with the time lag in the system  $\tau$  are shown in Figures 5(a) to 5(c). It can be seen clearly that for all the three cases, the stability boundary predicted with the small time lag assumption does not match very well with the exact stability boundary of the delayed system. The curves approximately match when the time lag ( $\tau$ ) is very small.

However, the match deteriorates very fast with an increase in the time lag ( $\tau$ ). Note from Figure 5(b) that the small time lag assumption breaks down even at values of time lag like  $\tau = 0.2$ . Hence it is important to relax the small time lag assumption, as the typical mass flow rates encountered in experiments [3] are in the range 0.5 – 3 gm/s, which correspond to  $\tau$  values between 0.05 – 0.3 for the experimental configuration described by Matveev [3].

#### 4.2. Effect of heater power

The effect of varying the non-dimensional heater power ( $K$ ) on the evolution of the system is analyzed with the bifurcation diagram as shown in Figure 6(a). Nondimensional heater power can be increased by increasing the electrical power supplied to the heater [23] and it represents an increase in the driving force given to the system. Increased driving strives to destabilize the system. Therefore, for small values of  $K$ , the equilibrium is stable and all perturbations decay asymptotically to zero. Increasing  $K$  decreases the margin of stability of the flow and at a critical value of  $K$ , a pair of complex eigenvalues of the system cross over to the right half plane (Hopf bifurcation) and the system becomes linearly unstable resulting in an oscillating flow pattern in the tube.

The variation of  $|U_1|$  with  $K$  is shown in Figure 6(a). The empty circles indicate unstable solutions and filled circles indicate stable solutions. A limit cycle is first obtained by varying the parameter near the Hopf point and iterating using a Newton's scheme. As discussed earlier, the bifurcation is subcritical and the resulting small-amplitude limit cycles close to the Hopf point are unstable. These unstable limit cycles are obtained using numerical continuation of the limit cycle and they coexist with the stable equilibrium. This unstable branch of limit cycles further undergoes a fold or turning point bifurcation and gains stability [29].

The bifurcation diagram for the variation of the non-dimensional heater power is obtained for various values of time lag  $\tau$  in the interval [0.2, 0.8] and all the results are plotted along with the stability boundary for the system as a 3-D plot in  $(\tau, K, |U_1|)$  in Figure 6(b). From this 3-D bifurcation diagram, we can also obtain the 2-D bifurcation diagram involving the limit cycle amplitude variation with the time lag  $\tau$  for a given value of  $K$ .

#### 4.3. Effect of damping

To study the effect of the variation of the amount of damping present in the system on the response of the system, one of the damping coefficients ( $c_1$ ) of the mode dependent damping model is varied. Change in the damping of the system can be achieved in experiments by changing the end conditions of the duct. As expected, increased

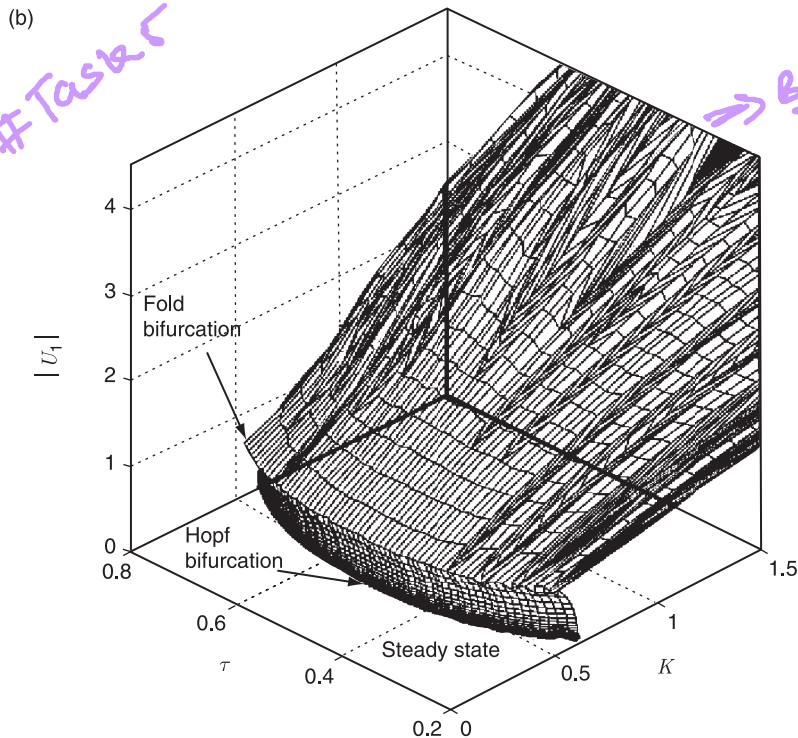
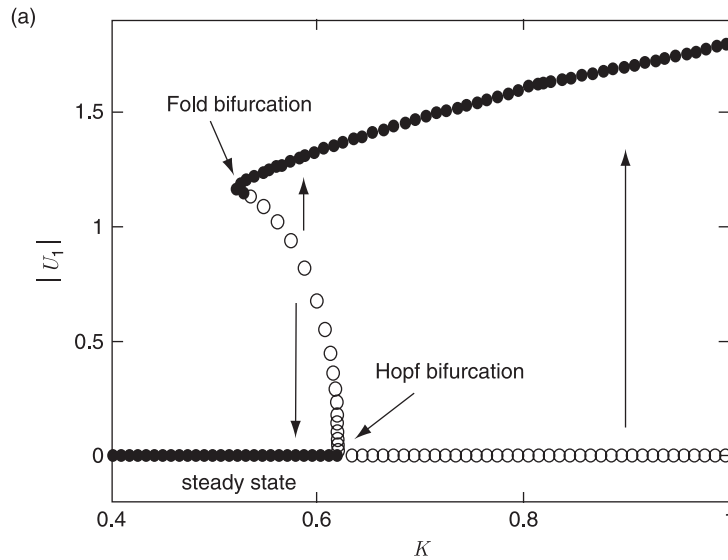


**Figure 6:** (a) Bifurcation plot for variation of non-dimensional heater power  $K$ . The other parameter values of the system are  $c_1 = 0.1$ ,  $c_2 = 0.06$ ,  $x_f = 0.3$  and  $\tau = 0.2$ . (b) 3D plot of bifurcation plot of non-dimensional heater power  $K$  for varying values of time lag  $\tau$  with the other parameters of the system  $c_1 = 0.1$ ,  $c_2 = 0.06$  and  $x_f = 0.3$ .

damping has a stabilizing effect on the dynamics of the system since the equilibrium is stable for any  $\tau$  for larger damping coefficients and lowering of damping might lead to instability depending on the time lag  $\tau$  as shown in figure 5(b).

For a fixed time lag, there exists a critical value of  $c_1$  below which all perturbations grow to limit cycles and above which there exists a region wherein large amplitude perturbations grow to limit cycles and small perturbations decay to the equilibrium as shown in Figure 7(a). The critical value of the damping coefficient  $c_1$  and the bifurcation diagrams has been obtained for various values of the time lag  $\tau$  again and the results are plotted as a 3-D plot in Figure 7(b). A 2-D projection of this plot on the  $(\tau, c_1)$  plane gives us the linear stability boundary (Hopf points also shown in Figure 5(b)) as well as the nonlinear stability boundary (fold points). The region enclosed between them gives us the bistable region to be discussed in more detail in subsequent subsections.

#### 4.4. Effect of heater location

The location of the heat source ( $x_f$ ) also has a very significant effect on the dynamics of the system and is achieved by placing the heater at different locations along the length of the duct. The stability of the system depends on the location of the heater along the duct in a non-trivial manner. When the location of the heater along the duct is varied from the upstream open end, the system is initially linearly stable. At a critical value of the heater location  $x_{f1}$ , a pair of complex eigenvalues crosses over to the right half plane and the system becomes linearly unstable. With further change in the location of the heater, the system remains linearly unstable till  $x_{f2}$ , when another Hopf bifurcation is observed in which a pair of complex eigenvalues crosses from the right half plane to the left half plane and the system regains linear stability as also shown in Figure 5(c).

The bifurcation plot for the variation of heater location ( $x_f$ ) shows subcritical Hopf bifurcation at both the locations along the duct length corresponding to the Hopf bifurcation as shown in Figure 8. The stable branch of limit cycles arising from the turning point bifurcations of the two branches of unstable limit cycles emanating from the Hopf points merge smoothly such that the region of linear instability is completely bounded by a single branch of stable limit cycles. Any initial condition within the linearly unstable region will asymptotically reach the corresponding stable limit cycle. An initial condition within the subcritical region will either decay asymptotically or reach the corresponding limit cycle based on whether it is above or below the stable manifold of the unstable limit cycles. The amplitude of limit cycle is seen to be a strong function of the location of the heater and is seen to increase with an increase in the heater location from the open upstream condition.

#### 4.5. Bistability regions

As discussed in section 3.2, there are regions of bistability for parameter ranges where the system can reach an equilibrium solution or a limit cycle depending on the initial conditions. This bistable region lies between the linear stability boundary given by the Hopf point and the nonlinear stability boundary given by the fold points. For the unstable region bounded by the Hopf bifurcation points, the system is unstable to any



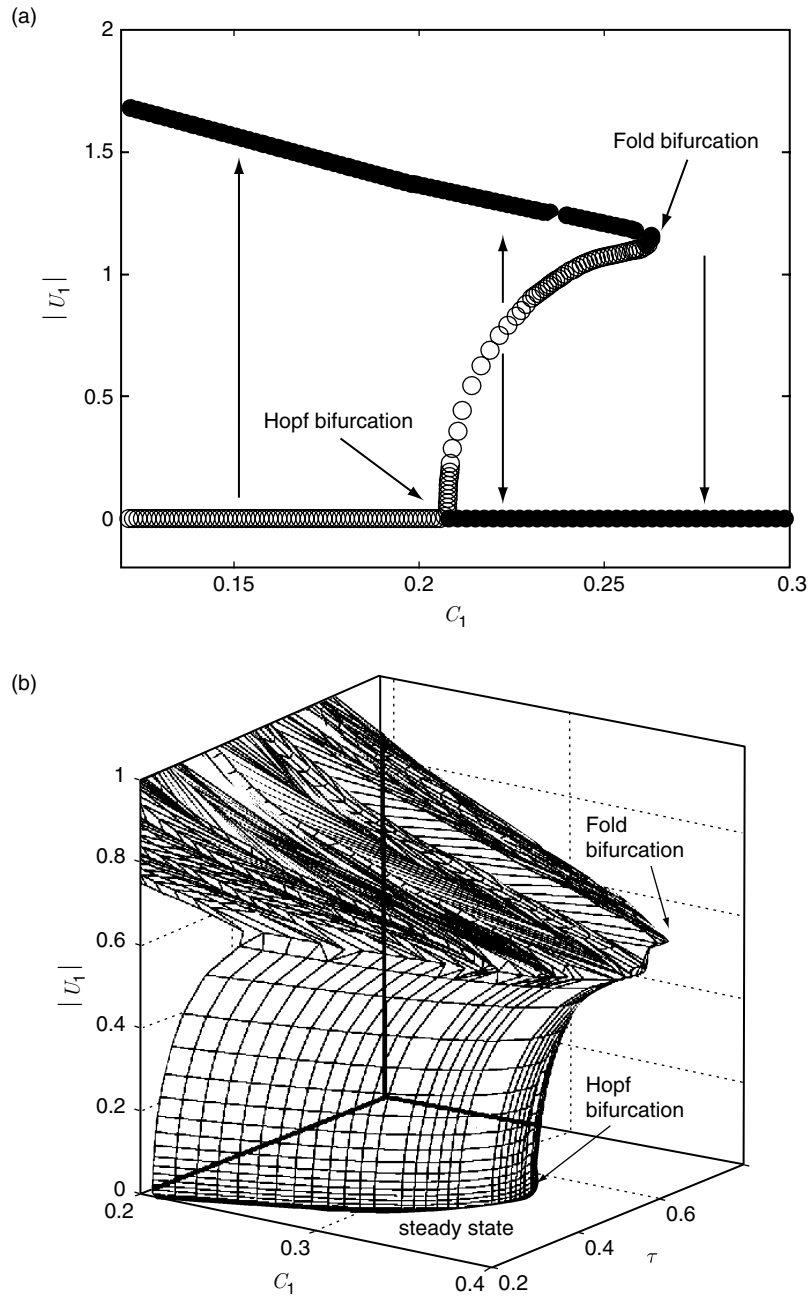


**Figure 7:** (a) Bifurcation plot for variation of damping coefficient  $c_1$ . The other parameter values of the system are  $c_2 = 0.06$ ,  $K = 1$ ,  $x_f = 0.3$  and  $\tau = 0.2$  (b) 3D plot of bifurcation plot of damping coefficient for varying values of time lag  $\tau$  with the other parameters of the system  $c_2 = 0.06$ ,  $K = 1$  and  $x_f = 0.3$ .

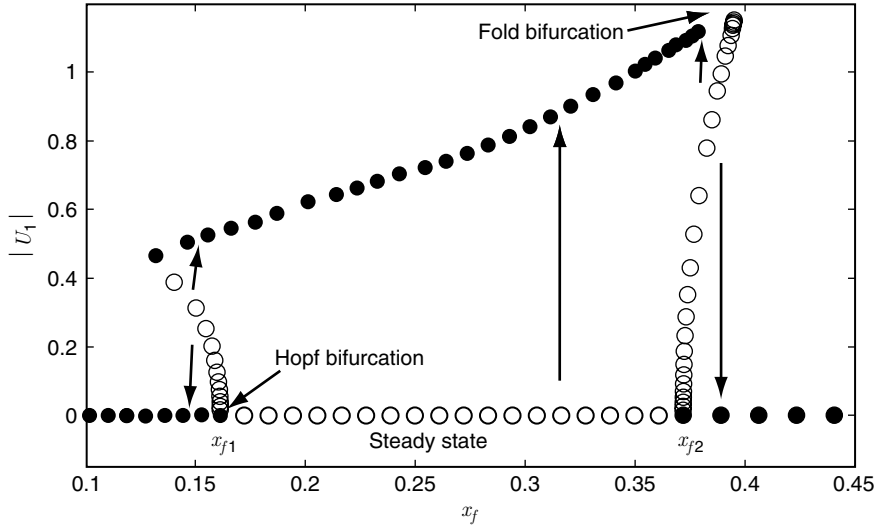


**Figure 8:** Bifurcation plot for variation of location of heater ( $x_f$ ). The other parameter values of the system are  $c_1 = 0.1$ ,  $c_2 = 0.06$ ,  $K = 0.8$  and  $\tau = 0.2$ .

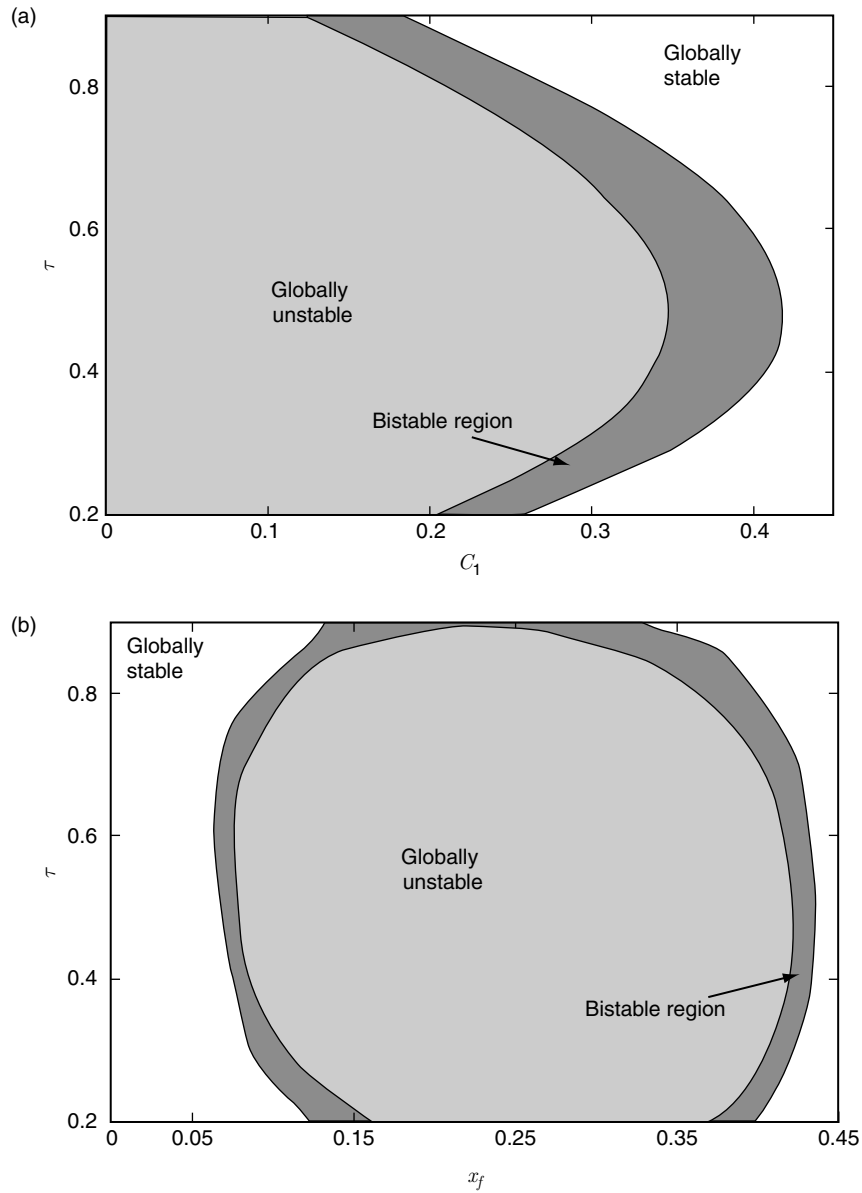
perturbation and hence, this region is termed as a globally unstable region. The system is globally stable to any perturbations for parameters in the region outside the nonlinear stability boundary (fold points) and this is called the region of global stability [30]. Thus the linear and nonlinear stability boundaries divide the parameter plane into three regions. The globally unstable region is shaded with light grey, the region filled with dark grey correspond to region of bistability and the white region represents globally stable region in Figure 9.

Figure 9 shows the bistable regions along with the globally stable and unstable regions for variations of the damping coefficient ( $c_1$ ) and the heater location ( $x_f$ ) as functions of the time lag  $\tau$ . From Figure 9(a), we can observe that the bistable region in the damping coefficient  $c_1$  first increases with an increase in  $\tau$ , reaches a maximum value and starts decreasing thereafter.

In contrast, the bistable region in the parameter  $x_f$  first decreases with an increase in the time lag  $\tau$  and increases after reaching a minimum value at a certain critical value of  $\tau$  as shown in Figure 9(b). The extremum value of the bistable regime typically appears at the parameter value  $\tau$  at which the other parameter value corresponding to the linear stability boundary reaches an extremum itself.

#### 4.6. Characterizing dynamical behavior through time evolutions

The linear stability boundaries obtained for the simultaneous variation of various parameters with the time lag of the system were given in Figure 5. The variation of the time lag of the system can be obtained in experiments by changing the mean flow rate of air through the duct. However, the most relevant parameters which could be varied in an experiment are



**Figure 9:** Region of bistability obtained for the bifurcation between (a) damping coefficient ( $c_1$ ) and time lag ( $\tau$ ) with the other system parameters being  $c_2 = 0.06$ ,  $K = 1$  and  $x_f = 0.3$  (b) heater location ( $x_f$ ) and time lag ( $\tau$ ) with the other system parameters being  $c_1 = 0.1$ ,  $c_2 = 0.06$  and  $K = 0.8$ .

the heater location along the duct ( $x_f$ ) and the heater power [3] ( $K$ ). The stability boundary for the simultaneous variation of these two parameters is given in Figure 10.

This figure shows that the linear stability boundary crosses itself many times to form loops. Along the direction of increasing power for a given heater location, linear stability is lost after the first crossing of the stability boundary. Further crossings lead to other pairs of eigenvalues moving to the right half plane. Accordingly the regions enclosed by the loops in the stability curves have two or more pairs of unstable eigenvalues and hence indicate the occurrence of interesting dynamical behavior in these parameter combinations e.g. points  $A$  to  $F$ . At these parameter combinations complicated dynamical behavior such as quasiperiodicity, co-existing multiple attractors, chaos etc. may be observed.

In this subsection we will characterize the dynamical behavior of the system through time evolutions corresponding to some typical points marked  $A$  to  $F$  in the linearly

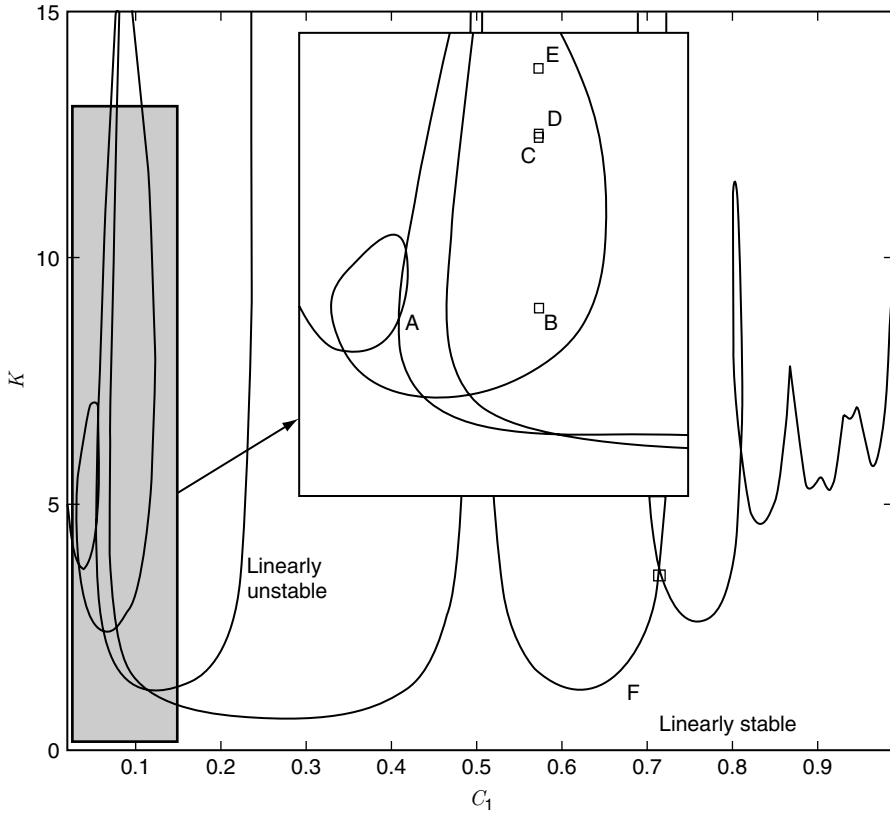


**Figure 10:** Linear stability boundary obtained for location of heater ( $x_f$ ) and non-dimensional heater power ( $K$ ) with the other system parameters being  $c_1 = 0.1$ ,  $c_2 = 0.06$  and  $\tau = 0.2$ . Time evolutions at points marked from  $A$  to  $F$  are studied to observe the asymptotic behavior of the system at these parameter values.

unstable region of the Figure 10 and its inset. These are chosen to represent more complicated solutions and situations than those already discussed in this work.

Shown in Figure 11(a) is the system evolution for parameters corresponding to the point *A*. At this point, we see that the system has an asymptotic behavior in which the amplitude of the limit cycle is modulated periodically. This type of regular amplitude

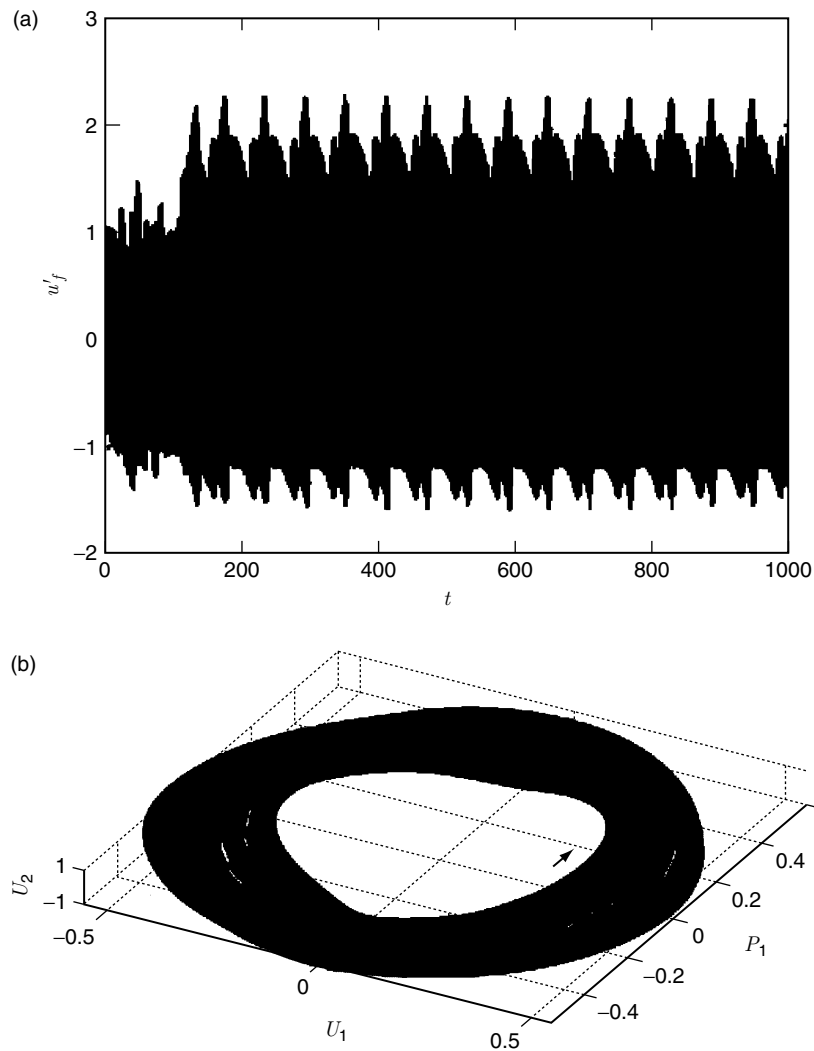


**Figure 11:** Quasiperiodic evolution is seen from the phase plots of system near point *A* with the system parameters being  $c_1 = 0.1$ ,  $c_2 = 0.06$ ,  $K = 4.5$ ,  $x_f = 0.05332$  and  $\tau = 0.2$ . (a) Time evolution with periodically modulated evolution and (b) Phase plot of evolution from 11 (a) showing a quasiperiodic orbit. Arrow indicates direction of evolution of the system.

modulation of the time series is related to the beating phenomena and represents a quasiperiodic solution. Figure 11(b) shows a 3-D projection of the phase portrait corresponding to the quasiperiodic solution. It can be clearly observed from Figure 11(b) that the trajectory stays on a torus and completely fills out its surface. We also observe chaotic solutions for our system for specific choice of parameter values. One of the routes to chaos is the period-doubling route to chaos wherein periodic solutions with longer and longer time-periods are observed with a change in some typical parameter till aperiodic solutions appear [31]. This particular route to chaos is observed as parameters are varied from points *B* through *E*. These points are chosen such that they lie in the direction of increasing heater power at a given heater location as shown in Figure 10. The phase plot of the evolution after the loss of linear stability at point *B* shows a limit cycle as given in Figure 12(a). Further increase in the nondimensional heater power to point *C* and *D* causes limit cycles with periods that are twice and four times the time-period corresponding to point *B*, respectively. The phase plots of these limit cycles are shown in

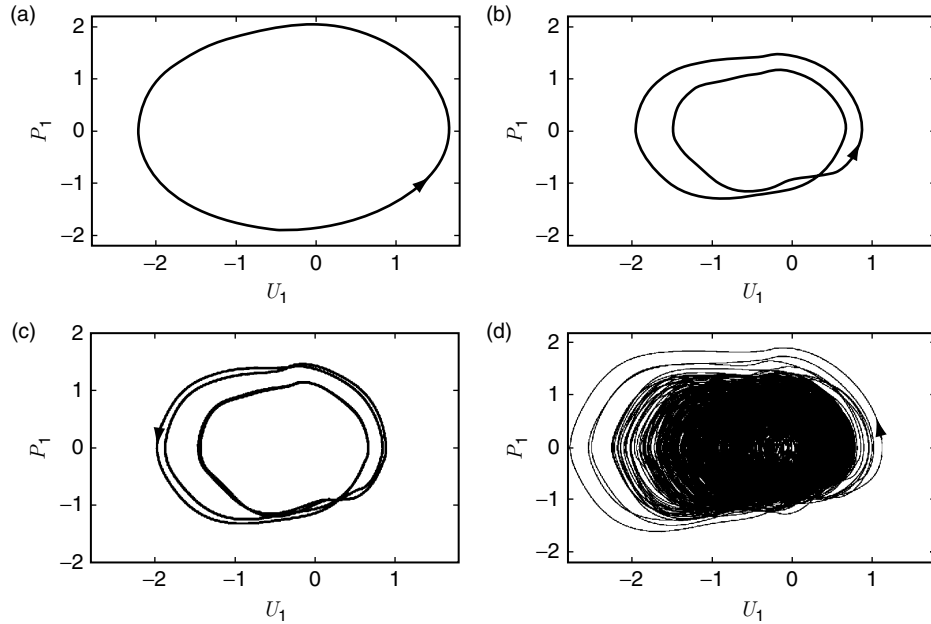


**Figure 12:** Period doubling route to chaos is seen from the phase plots of system at points *B* through *E* with the system parameters being  $c_1 = 0.1$ ,  $c_2 = 0.06$ ,  $x_f = 0.1$  and  $\tau = 0.2$ . Arrow heads indicate direction of evolution of system, (a) Phase plot at  $K = 4$ . A limit cycle of period 1 is obtained, (b) Phase plot at  $K = 10$ . A limit cycle of period 2 is obtained, (c) Phase plot at  $K = 10.1$ . A limit cycle of period 4 is obtained and (d) Phase plot at  $K = 12$ . The phase plot shows no discernable periodic behavior and trajectory moves all over the phase plot.

Figures 12(b) and (c) wherein the simple closed curve corresponding to the limit cycle in Figure 12(a) transforms into a closed curve which intersects itself once and twice respectively in this projection. With a sufficient increase in the heater power to point  $E$ , the system evolution becomes highly aperiodic (chaotic), and the trajectory is seen to fill almost an area in the phase space as shown in Figure 12(d).

Figure 13 shows that the time evolution of the system at point  $F$  with two different initial conditions gives two different asymptotic behavior. Time evolution at  $F$  with initial condition  $U_1 = 1.5$ ,  $U_i = 0$ ,  $\forall i \neq 1$  and  $P_i = 0$ ,  $\forall i = 1, \dots, N$  evolves into a complicated quasiperiodic attractor with a large magnitude of the total velocity fluctuation as shown in Figure 13(a). The frequency content of this attractor is shown in Figure 13(c) wherein the phase space projection of the solution on the first acoustic mode  $U_1$  and  $P_1$  is also shown in the inset. The arrow indicates the direction of evolution of the system in the phase plot. A second frequency close to zero is distinctly visible along with the major frequency at around 0.5 and its harmonics.

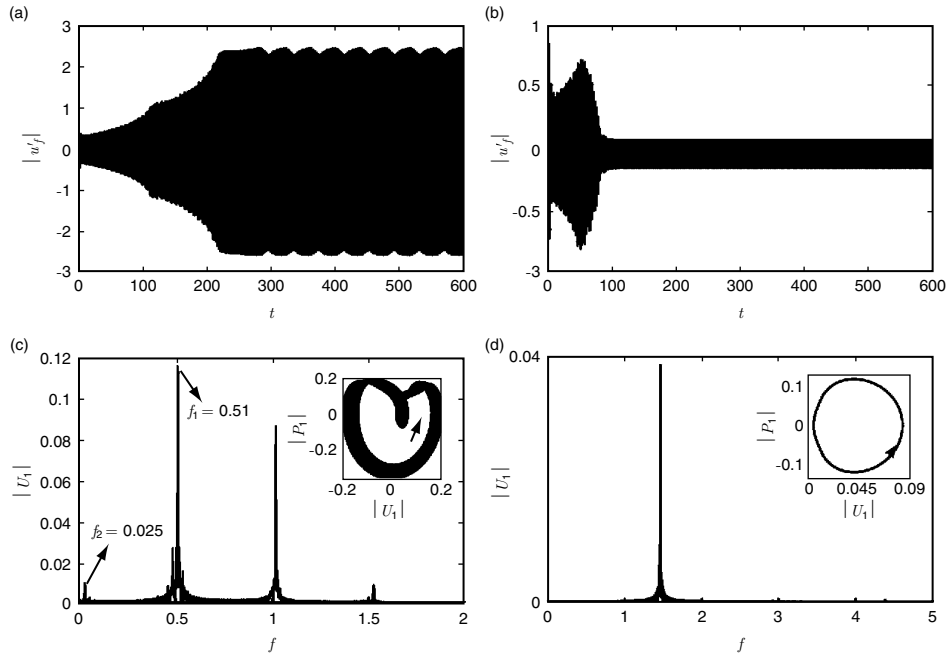


**Figure 13:** Coexisting multiple attractors obtained with different initial conditions at point  $F$  from Figure 10 with the system parameters being  $c_1 = 0.1$ ,  $c_2 = 0.06$ ,  $K = 3.5$ ,  $x_f = 0.7141$  and  $\tau = 0.2$ . (a) Time evolution from initial condition  $U_1 = 1.5$ ,  $U_i = 0$ ,  $\forall i \neq 1$  and  $P_i = 0$ ,  $\forall i = 1, \dots, N$ , (b) Time evolution from initial condition  $U_1 = 0.5$ ,  $U_i = 0$ ,  $\forall i = 1$  and  $P_i = 0$ ,  $\forall i = 1, \dots, N$ , Frequency content of evolution (c) from Figure 11(a) and (d) from Figure 11(a) with insets showing the phase plot.

The time evolution with a different initial condition of  $U_1 = 0.5$ ,  $U_i = 0 \ \forall \ i \neq 1$  and  $P_i = 0 \ \forall \ i = 1, \dots, N$  however reaches a small amplitude limit cycle where the third mode is primarily unstable as shown in Figure 13(b). The frequency content of this limit cycle shown in Figure 13(d) clarifies that the third mode with a fundamental frequency of around 1.5 is unstable. At a given heater power level and heater location, we thus observe the coexistence of two different attractors. One of them is a low amplitude limit cycle and the other is a high amplitude quasiperiodic solution. Thus, a given system can produce two qualitatively as well as quantitatively different noise levels.

Thus, we have seen that for different system configurations, the dynamics of the system model can exhibit complicated dynamical behaviors such as coexisting attractors, quasiperiodicity, complicated limit cycles with increasing time-periods and chaotic solutions. These behaviors have been observed in experiments: ducted premixed flame [32] and laboratory combustor [33].

#### 4.7. Comparison with experimental results

Experimental determination of the stability boundaries and bifurcation behavior of a horizontal Rijke tube have been performed by Matveev [3, 4] and Song *et al.* [34]. Matveev [4] obtained the stability boundaries for a horizontal Rijke tube and also reported hysteresis at the stability boundary. Song *et al.* [34] also obtained linear stability boundary and matched their results with Matveev [4]. In both the papers, the linear stability boundaries were obtained for the simultaneous variation of heater power and mass flow rate at different locations along the Rijke tube.

Changes in heater power leads to changes in the non-dimensional heater power ( $K$ ). The effect of heater power and mass flow rate in determination of  $K$  is as given in Eqn (11). Increasing heater power increases the temperature of the wire and affects  $K$  while increasing mass flow rate increases  $u_0$  thereby decreasing  $K$ . The effect of changing mass flow rate affects both the non-dimensional power  $K$  and the time lag  $\tau$  through changes in the mean velocity. Variation in  $K$  occurs according to the Eqn (11) while time lag is related to the mean velocity through the quasi-steady approximation given by Lighthill [35]

$$\tau = \frac{0.2d_w}{u_0} \left( \frac{c_0}{l} \right). \quad (14)$$

The additional factor of  $(c_0/l)$  has been included to non-dimensionalize the time lag. Damping coefficients,  $c_1$  and  $c_2$  are calculated using the formula given in Matveev [4]. The stability boundaries obtained at two different heater locations from Matveev's experiments are shown as + in Figure 14. The corresponding numerical results from the present study are denoted with solid lines in the same figure. Figure 14 (a) is the linear stability boundary when the heater is placed at one-quarter of the duct length. At this location, the frequency close to the fundamental mode of the duct becomes unstable. Figure 14 (b) shows the linear stability boundary when the heater is placed at 5/8<sup>th</sup> of the duct length where the frequency close to the second mode of the duct becomes



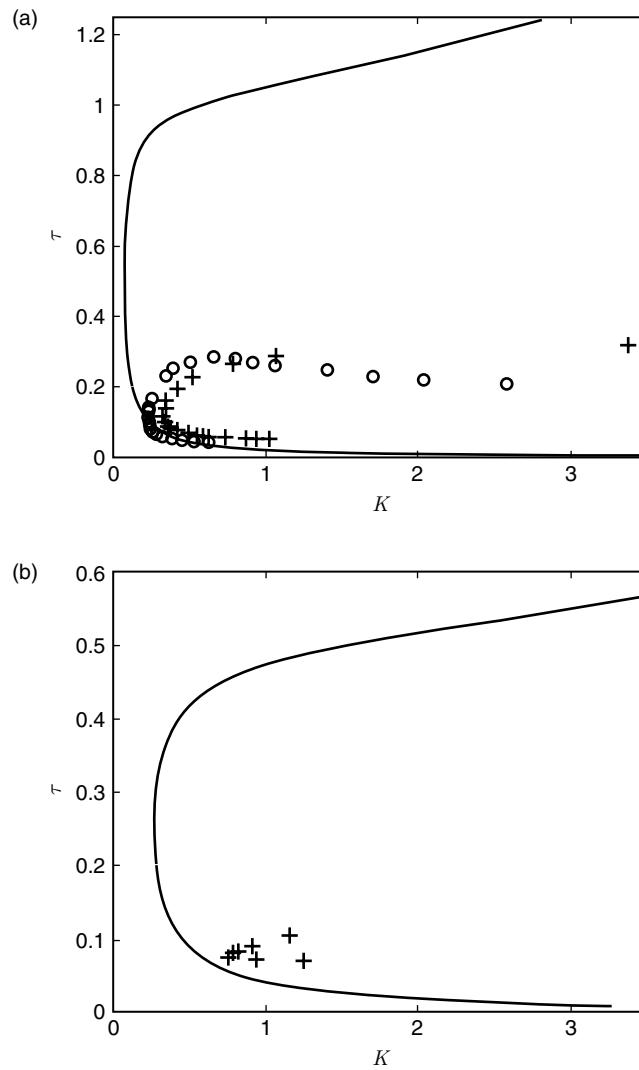


**Figure 14:** Comparison of linear stability boundary between numerical (—) and experimental data from Matveev [4] (+ + +) and Song *et al.* [34] (o o o) for the simultaneous variation of non-dimensional power ( $K$ ) and time lag ( $\tau$ ) when the heater location is (a)  $x_f = 1/4$  and (b)  $x_f = 5/8$ . The other system parameters are  $c_1 = 0.028$ ,  $c_2 = 0.0001$ .

unstable. In both the cases the linear stability boundary predicted has the same trend as the experimental observations.

Matveev [3] also reported hysteresis at the stability boundary for different mass flow rates. Results obtained from his experiments are shown as  $\times$  and  $\circ$  in the Figures 15 (a)

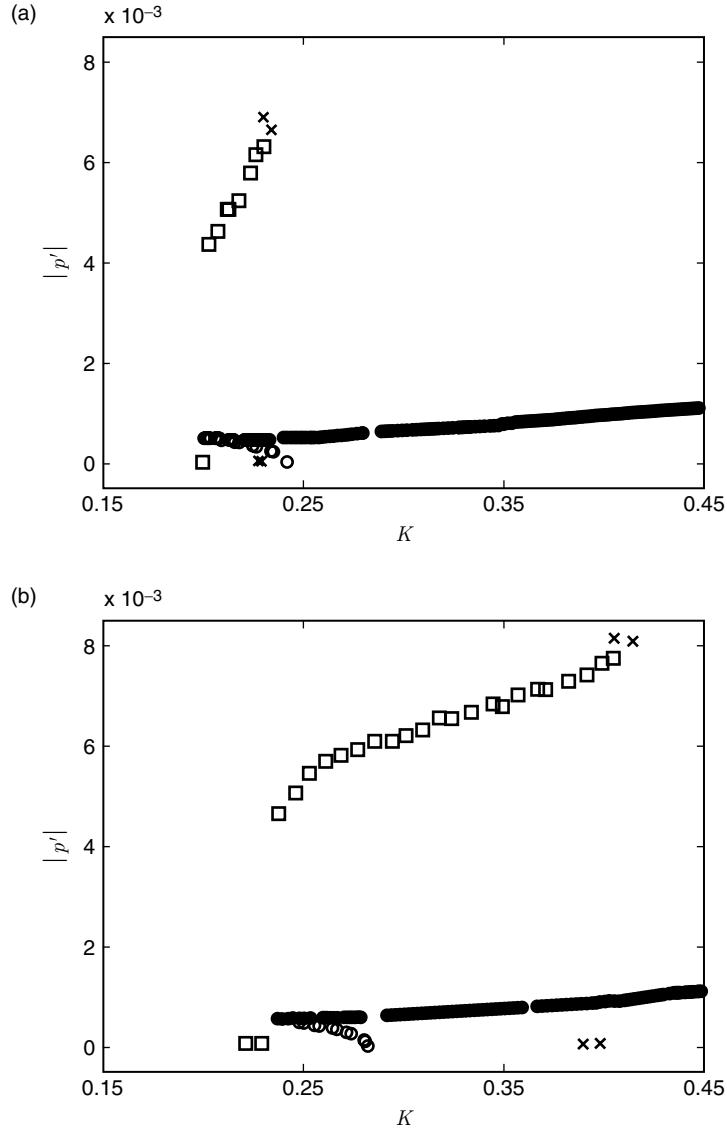


**Figure 15:** Comparison of bifurcation behavior for the variation of non-dimensional heater power ( $K$ ) between numerical models and experiment,  $\circ$  are the unstable limit cycles and  $\bullet$  are the stable limit cycles predicted by the current model for (a)  $\tau = 0.08$  or  $\dot{m} = 2.75$  gm/sec and (b)  $\tau = 0.07$  or  $\dot{m} = 3.15$  gm/sec.  $\times$  are experimental data points obtained when power was increased and  $\square$  are data points obtained when power was reduced for  $c_1 = 0.028$ ,  $c_2 = 0.0001$  and  $x_f = 0.25$ .

and (b). In order for comparison with experimental data, the measure chosen in the bifurcation plots is  $|p'|$ , the amplitude of the acoustic pressure. In the plot,  $\times$  indicate values acquired during increase of power and  $\square$  correspond to data for the decrease in power. The numerically calculated bifurcation plots for the same system parameters are compared with the experimental data for two different mass flow rates. In both the cases, the limit cycle amplitudes predicted are much lower than the observed values.

The under prediction of limit cycle amplitudes can be attributed to the following reasons. A mesh type electrical heater is used in experiments [3] while the present model assumes the flow over a single cylinder. However, the heat transfer characteristics of a single cylinder is significantly different from that of a mesh [36]. A constant speed of sound is assumed throughout the tube in the present model. However, the presence of the heater causes a higher downstream temperature. This could have a noticeable effect on linear stability and oscillation amplitude by modifying the eigenfrequencies and mode shapes. Also, the present model assumes significant nonlinear effects when the amplitude of the velocity fluctuations exceed one-third of the steady state velocity. However, recent results for the nonlinear system identification of pulsatile flow over a cylinder [37] show that the effect of nonlinearity in the heat release rate response occurs only when the perturbation velocities exceed 1.5 times the steady state velocity. Due to the above reasons, the limit cycle amplitudes predicted by Heckl's correlation are lower than experimental results.

The numerically predicted Fold points are close to the experimental results while the Hopf point is over predicted in Figure 15 (a) and under predicted in Figure 15 (b). This shift in the Hopf point may be due to the presence of inherent noise in actual experiments. Uncertainties in the parameters is seen to affect the bifurcation behavior [38] while noise in the initial perturbation can cause sub-critical transition to instability [39] in the present Rijke tube model. A factor which possibly contributes to the mismatch is related to the uncertainties in the values of steady state parameters. The value of the damping coefficients ( $c_1$  &  $c_2$ ) used are currently calculated from the cold flow conditions [23]. However, these values could be different when the heater is turned on. Further investigations are required to determine the variation of the damping coefficients with temperature.

Another reason for the mismatch of the present model could be the use of a single time lag to obtain the response of the heater to velocity perturbations. Other investigations of the Rijke tube model which include multiple time lags [40] exhibit higher limit cycle amplitudes. Studies incorporating a modeling of the heat release rate using multiple time lags to better correspond to the experiments would be undertaken in our future work. The main objective of the present study was to demonstrate the use of the software DDE-BIFTOOL in a systematic analysis of these models. An encouraging outcome of the present study is that even with these simplifying assumptions, our model is seen to predict the trends in the linear stability boundaries and the bifurcation behavior of a Rijke tube which are reasonably close to the experimental results.

## 5. CONCLUSIONS

The dynamical behavior of a model for a horizontal Rijke tube has been studied using the method of numerical continuation. Linear stability boundary for the simultaneous variation of two parameters of the system are obtained. The stability predictions calculated by linearizing about the unperturbed state with small time lag are shown to be not accurate.

The nonlinear stability boundary and the regions of bistability where the system can reach one or two possible asymptotic states are also obtained. Using the linear and nonlinear stability boundaries, regions of global stability, global instability and regions of potential instability are identified for the Rijke tube model. It is seen that only subcritical Hopf bifurcations are possible for the model considered to represent the behavior of the Rijke tube. The stability boundaries obtained are complicated, and interesting dynamical behavior such as co-existing limit cycles, quasiperiodic behavior and period doubling route to chaos are observed.

Linear stability boundaries and bifurcation plots obtained from numerical continuation are compared with experimental data. Trends of the numerically obtained linear stability boundaries are similar to experimental results. However, the numerical model under predicts the amplitude of the stable limit cycles observed in experiments. In summary, reduced order models of physical systems with explicit time delays can be studied in detail using the method of numerical continuation to identify stability boundaries, to obtain bifurcation plots and to examine their possible dynamical behavior.

## 6. ACKNOWLEDGMENTS

This work was funded by the Department of Science & Technology (DST), India. The authors wish to acknowledge Dr. M. K. Verma for his valuable suggestions and Mr. Ashesh Saha (IIT Kanpur) for guidance in using DDE-BIFTOOL.

## REFERENCES

- [1] K. McManus, T. Poinso and S. Candel, A review of active control of combustion instabilities, *Progress in Energy and Combustion Science*, 1993, 19, 1–29.
- [2] J. M. Wicker, W. D. Greene, S. I. Kim and V. Yang, Triggering of longitudinal combustion instabilities in rocket motors: nonlinear combustion response, *Journal of Propulsion & Power*, 1996, 12, 1148–1158.
- [3] K. I. Matveev, Thermo-acoustic instabilities in the Rijke tube: Experiments and modeling, Ph.D. thesis, 2003, California Institute of Technology, Pasadena.
- [4] K. I. Matveev and F. E. C. Culick, A study of the transition to instability in a Rijke tube with axial temperature gradient, *Journal of Sound & Vibration*, 2003, 264, 689–706.
- [5] K. Balasubramanian and R. I. Sujith, Thermoacoustic instability in a Rijke tube: Non-normality and nonlinearity, *Physics of Fluids*, 2008, 20, 044103.

- [6] J. A. Carvalho, M. A. Ferreira, C. Bressan and L. G. Ferreira, Definition of heater location to drive maximum amplitude acoustic oscillations in a Rijke tube, *Combustion & Flame*, 1989, 76, 17–27.
- [7] Y. P. Kwon and B. H. Lee, Stability of the Rijke thermoacoustic oscillation, *Journal of the Acoustical Society of America*, 1985, 78, 1414–1420.
- [8] C. C. Hantschk and D. Vortmeyer, Numerical simulation of self-excited thermoacoustic instabilities in a Rijke tube, *Journal of Sound and Vibration*, 1999, 227, 511–522.
- [9] S. Mariappan and R. I. Sujith, Modeling nonlinear thermoacoustic instability in an electrically heated Rijke tube, 48th AIAA Aerospace Sciences Meeting Including the New Horizons Forum and Aerospace Exposition, 2010, 2010–25.
- [10] M. A. Heckl, Nonlinear acoustic effects in the Rijke tube, *Acustica*, 1990, 72, 63–71.
- [11] C. C. Jahnke and F. E. C. Culick, Application of dynamical systems theory to nonlinear combustion instabilities, *Journal of propulsion and power*, 1994, 10, 508–517.
- [12] N. Ananthkrishnan, S. Deo and F. E. C. Culick, Reduced-order modeling and dynamics of nonlinear acoustic waves in a combustion chamber, *Combustion Science and Technology*, 2005, 177, 221–248.
- [13] J. P. Moeck, M. R. Bothien, S. Schimek, A. Lacarelle and C. O. Paschereit, Subcritical thermoacoustic instabilities in a premixed combustor, 14th AIAA/CEAS Aeroacoustics Conference, 2008, 2946.
- [14] B. Hasselblatt, B. Fiedler and A. Katok, Handbook of dynamical systems, 2002, Elsevier Publishing, Amsterdam.
- [15] E. L. Allgower and K. Georg, Introduction to Numerical Continuation Methods, 2003, Society for Industrial and Applied Mathematics, Philadelphia.
- [16] V. S. Burnley, Ph.D. Dissertation: Nonlinear Combustion Instabilities and Stochastic Sources, 1996, California Inst. of Technology, Pasadena.
- [17] C. A. Fannin, W. R. Saunders, M. A. Vaudrey, B. Eisenhower and U. Vandsburger, Identification of a model for thermoacoustic instabilities in a Rijke tube, *IEEE Transactions on control systems technology*, 2002, 10, 490–502.
- [18] K. Engelborghs and D. Roose, Numerical computation of stability and detection of Hopf bifurcations of steady state solutions of delay differential equations, *Advances in Computational Mathematics*, 1999, 10, 271–289.
- [19] K. Engelborghs, T. Luzyanina and D. Roose, Numerical bifurcation analysis of delay differential equations using dde-biftool, *ACM Transactions on Mathematical Software*, 2002, 28, 1–21 .
- [20] F. Nicoud, L. Benoit, C. Sensiau and T. Poinsot, Acoustic Modes in Combustors with Complex Impedances and Multidimensional Active Flames, *AIAA Journal*, 2007, 45-2, 426–441.

- [21] L. V. King, On the Convection of Heat from Small Cylinders in a Stream of Fluid: Determination of the Convection Constants of Small Platinum Wires, with Applications to Hot-Wire Anemometry, *Proceedings of the Royal Society of London. Series A, Containing Papers of a Mathematical and Physical Character*, 1914, 90, 271–289.
- [22] B. T. Zinn and M. E. Lores, Application of the Galerkin method in the solution of non-linear axial combustion instability problems in liquid rockets, *Combustion Science & Technology*, 1971, 4, 269–278.
- [23] K. I. Matveev, A Model for combustion instability involving vortex shedding, *Combustion Science and Technology*, 2003, 175-6, 1059–1083.
- [24] H. M. Gibbs, F. A. Hopf, D. L. Kaplan and R. L. Shoemaker, Observation of Chaos in Optical Bistability, *Phys. Rev. Lett.*, 1981, 46-7, 474–477.
- [25] Garcia-Ybarra, P. L., Antoranz, J. C., Sankovitch, V. and Castillo, J. L., Experimental evidence of self-excited relaxation oscillations leading to homoclinic behavior in spreading flames, *Phys. Rev. E*, 1994, 49-6, 5225–5229.
- [26] A. Saha, B. Bhattacharya and P. Wahi, A comparative study on the control of friction-driven oscillations by time-delayed feedback, *Nonlinear Dynamics*, 2009, 60, 15–37.
- [27] T. Kalmar-Nagy, G. Stepan and F. C. Moon, Subcritical Hopf bifurcation in the delay equation model for machine tool vibrations, *Nonlinear Dynamics*, 2001, 26, 121–142.
- [28] P. Wahi and A. Chatterjee, Regenerative tool chatter near a codimension 2 Hopf point using multiple scales, *Nonlinear Dynamics*, 2005, 40, 323–338.
- [29] V. Ajjarapu, Computational techniques for voltage stability assessment and control, 2006, Springer, New York.
- [30] S. H. Strogatz, Nonlinear Dynamics and Chaos: with applications to Physics, Biology, Chemistry and Engineering, 2000, Westview Press, Colorado.
- [31] G. L. Baker and J. P. Gollub, Chaotic Dynamics: an introduction, 1990, Cambridge University Press, Cambridge.
- [32] L. Kabiraj, A. Saurabh, P. Wahi and R. I. Sujith, Experimental study of thermoacoustic instability in ducted premixed flames: periodic, quasi-periodic and chaotic oscillations, Proceedings of n31 - Int'l Summer School and Workshop on Non-Normal and Nonlinear Effects in Aero- and Thermoacoustics, Munich, 2010.
- [33] J. D. Sterling and E. E. Zukowski, Nonlinear Dynamics of Laboratory Combustor Pressure Oscillations, *Combustion Science and Technology*, 1991, 77–4, 225–238.
- [34] Woo-Seog Song, Seungbae Lee, Dong-Shin Shin and Yang Na, Thermo-acoustic instability in the Horizontal Rijke tube, *Journal of Mechanical Science & Technology*, 2006, 20–6, 905–913.
- [35] M. J. Lighthill, The Response of Laminar Skin Friction and Heat Transfer to Fluctuations in the Stream Velocity, *Proceedings of the Royal Society of London. Series A, Mathematical and Physical Sciences*, 1954, 224, 1–23.

- [36] S. Sen, S. Mittal and G. Biswas, Steady separated flow past a circular cylinder at low Reynolds numbers, *Journal of Fluid Mechanics*, 2009, 620, 89–119.
- [37] F. Selimefendigil, R. I. Sujith and W. Polifke, Identification of heat transfer dynamics for nonmodal stability analysis of thermoacoustic systems, AIP conference proceedings, 2010, 605–608.
- [38] V. Nair, S. Sarkar and R. I. Sujith, Uncertainty Quantification of Subcritical Bifurcation in a Rijke Tube, 16th AIAA/CEAS Aeroacoustics conference, 2010, 2010–3858.
- [39] I. C. Waugh, M. P. Juniper and M. Geuss, Triggering in a thermoacoustic system with stochastic noise, Proceedings of n31 - Int'l Summer School and Workshop on Non-Normal and Nonlinear Effects in Aero- and Thermoacoustics, Munich, 2010.
- [40] F. Selimefendigil and W. Polifke, A Frequency domain system model with coupled modes for limit cycle prediction of thermoacoustic systems, Proceedings of n31 - Int'l Summer School and Workshop on Non-Normal and Nonlinear Effects in Aero- and Thermoacoustics, Munich, 2010.